Hindawi
Geofluids
Volume 2022, Article ID 1620624, 9 pages
https://doi.org/10.1155/2022/1620624

Research Article

Finite-Element Analysis on the Tensile Membrane Effect in Geogrid Reinforced Piled Embankment under Dynamic Loading

Yan Zhuang,[1,2] **Kangyu Wang**,[3] **Shunlei Hu**,[2] **Xidong Zhang**,[4] **and Xiaoyan Cui**[2]

[1]*School of Civil Engineering and Architecture, Hubei University of Technology, Wuhan 430068, China*
[2]*School of Civil Engineering, Southeast University, Nanjing 210096, China*
[3]*School of Civil Engineering, Zhejiang University of Technology, Hangzhou 310014, China*
[4]*College of Civil Engineering, Taiyuan University of Technology, Taiyuan 030024, China*

Correspondence should be addressed to Yan Zhuang; zhuangyan4444@hotmail.com

Received 6 June 2022; Revised 10 August 2022; Accepted 11 August 2022; Published 8 September 2022

Academic Editor: Xianwei Zhang

This study presented a numerical investigation of the tensile membrane effect in the geogrid reinforced piled embankment under dynamic loading. It has been found that the maximum sag of the geogrid was attained at the center of two adjacent piles, while localization of tensile force was observed at the corners of the pile caps. Under the dynamic loading, the sag and the strain of the geogrid increased when compared with the static loading, an increase of around 45.9% and 24% was, respectively, yielded for the sag and the strain of the geogrid. This increase of tension in the geogrid may mainly result from the degradation of the soil arching effect under dynamic loading. A parameter study was performed, and it showed that the tensile force in the geogrid increases with the rise of the embankment height, the clear pile spacing, and the tensile stiffness of the geogrid. However, the increase of the friction angle of the embankment fill led to a decrease in the tension in the geogrid, which may benefit from the improvement of the soil arching developed in the embankment fill. It was found that the tensile behavior of the geogrid was the most sensitive to the pile spacing. When pile spacing increased from 2.0 m to 3.0 m, the tensile force in the geogrid increased by about 248%.

1. Introduction

Highways usually have better quality, less congestion, and higher speed limits in comparison with ordinary roads, leading to more efficient transportation. In the construction of the piled embankment, introducing the geogrid reinforcement provides a reliable way to suppress the settlement and minimize the soil yielding above the pile cap [1–4].

The design of geogrid reinforced piled embankment may need to not exclusively consider the embankment stability and lateral sliding. The inclusion of geogrid reinforcement facilitates the vertical load transfers from the soft soil to the pile cap, benefiting from the so-called tensile membrane effect [5–7]. To ensure the safety of the geosynthetic reinforced piled embankment, the limit of the tensile strain of the reinforcement is frequently focused on in some design codes. The British design code (BS8006) [8] proposed a design method for estimating the arching effect based on the Hewlett and Randolph model [9], and a maximum limit of the tensile strain of the reinforcement was also given. The German design code [10] also suggested a method to calculate the maximum tensile strain of the reinforcement simply by considering the elastic behavior of the subsoil. Hu et al. [11] proposed a design method to determine the maximum strain of the reinforcement based on the German design code [10]. Zhuang and Ellis [12] calculated the tensile strain of the geogrid in the reinforced piled embankment by adopting the method proposed in the BS8006 [8] in which the calculated results were compared with the results from finite element analysis. A further study was conducted by Zhuang and Ellis [13] to investigate the tensile membrane effect caused by the overconsolidation of the subsoil in the

reinforced piled embankment. Van et al. [14, 15] modified the method in BS8006 in order to make the calculation more reliable. Zhuang et al. [16] developed a simplified design method to study the reinforced piled embankments. A 3D numerical model was validated using the centrifuge test results, and the tensile force of the reinforcement was calculated [17]. However, the tensile membrane effect of the reinforcement was not well investigated in the literature, particularly when dynamic loading is involved.

The tensile membrane effect in the piled embankment has not been widely investigated so far. Heitz et al. [18] conducted a large-scale model test of the geosynthetic reinforced piled embankment at a scale ratio of 1 : 3. It was concluded that the inclusion of geogrid enhanced the soil arching effect, considerably reducing the settlement at the top of the embankment. The strain in geogrid under dynamic loading might significantly increase, especially when the geogrid with low tensile stiffness was used. Han and Bhandari [19] explored the performance of pile embankments subjected to one cyclic loading. Chen et al. [20] investigated the tensile force of the reinforcement under dynamic loading based on a full-scale experimental study. They found that the tensile force increased slightly in the reinforcement placed above the subsoil, while the geogrid tension over the pile caps increased significantly. However, the geogrid tension under dynamic loading was qualitatively assessed and the discussion of the load transfer mechanism is absent. By performing large physical modeling tests, Liu et al. [21] stated that the loading frequency imposed a significant influence on the dynamic behaviors of the geosynthetic reinforced railway embankment. However, the loading conditions and the boundary conditions of the model test remain different from those of geosynthetic reinforced railway embankment. Therefore, further studies need to be carried out to comprehensively investigate the tensile membrane effect in the reinforced piled embankment under the traffic loading.

This study investigated the tensile membrane effect of the reinforcement in the reinforced piled embankment by using the 3D finite element (FE) technology [22]. The tensile force and the deflection of reinforcement are comprehensively analyzed to investigate the dynamic behaviors of the geosynthetic reinforced piled embankments. The variable pile spacings, the embankment heights, the geogrid stiffnesses, and the properties of embankment fill (i.e., friction angle) were studied and analyzed. The results were comparatively analyzed with the calculated results using the design methods developed by Zhuang and Ellis [12, 13].

2. Numerical Simulation

2.1. General Description. The three-dimensional (3D) finite element (FE) modeling of geogrid reinforced piled embankments under dynamic loading by using the software 'ABAQUS' (version 6.16) was presented. The study highlighted the dynamic behavior of the tensile membrane effect in the reinforced piled embankments. The cross-section of the numerical model was illustrated in Figure 1. A pavement was placed on the top of the embankment, including 0.15 m AC layer, 0.20 m base layer, and 0.25 m subgrade. The groundwater table was located at the top of the clay layer. The concrete piles were 0.3 m wide square with 1 m wide and 0.5 m thick cap. One layer of geogrid with the stiffness of J between 1 and 10 MN/m was adopted, which is set at 0.1 m above the roadbed. In this study, the pile spacing (s) was taken as 2.0 m, 2.5 m, and 3.0 m, and the embankment heights (h) were different, i.e., 3.5 m, 5.0 m, and 6.5 m. Much detailed information about the numerical model can be obtained in a previously published paper by Zhuang and Wang [23].

The displacements at the bottom and vertical boundaries of the model were set to zero. The phreatic level was set at the surface of the clay layer. Free drainage was simulated at the top and bottom boundaries using zero excess pore water pressure boundary conditions. The embankment fill was meshed using 8-node brick elements (C3D8), and its mechanical response was simulated with the Mohr-Coulomb model. The modified Cam-Clay model was applied to simulate the response of the subsoil. The piles and geogrid reinforcement adopt the linear elastic model. The geogrid reinforcement was modeled using membrane elements (M3D4), and only the tensile stiffness of the geogrid was considered with ignoring the bending stiffness. Assumed interface friction angle between geogrid and embankment fill (φ_{i1}) equal to the friction angle of embankment fill (φ_1'). According to Potyondy [24], the interface friction angle between pile and subsoil is assumed (φ_{i2}) equals $0.7\varphi_2'$, in which φ_2' is the friction angle of the subsoil. The properties of the materials used in the FE models are listed in Table 1. The bold values give the parameters in the standard case.

2.2. Simulation Procedure. In this study, the dynamic loading was a simple sine wave loading. Applied cyclic load on the pavement surface by using a subroutine called Dload. The total number of the repeated cycles of the cyclic loading acted on the pavement was 100 times.

3. Analysis of the Geogrid Membrane Effect under Dynamic Loading

3.1. Distribution of Sag and Tensile Force of the Geogrid Reinforcement. The sag of the geogrid is plotted in Figure 2. It has been shown that the general shape of the plots under both static and dynamic loadings shows quite similar features to that in some related studies performed by Halvordson et al. (see Figure 2) [25] and Zhuang and Ellis [12]. When compared with the static loading, the sag of geogrid under the dynamic loading condition increased by 23%.

Figure 3 shows the pulling force of the geogrid along with both the x and y directions. The results remain consistent with that in the studies conducted by Halvordson et al. [25] and Zhuang and Ellis [12]. The maximum tension in the geogrid occurs at the corners of the pile caps. The tensile force in the geogrid is approximately 1.24 times of that under the static loading condition.

3.2. Variation of Sag (δ) and Strain (ε) of Geogrid under Varied Stiffnesses. Figure 4 illustrates the settlement and

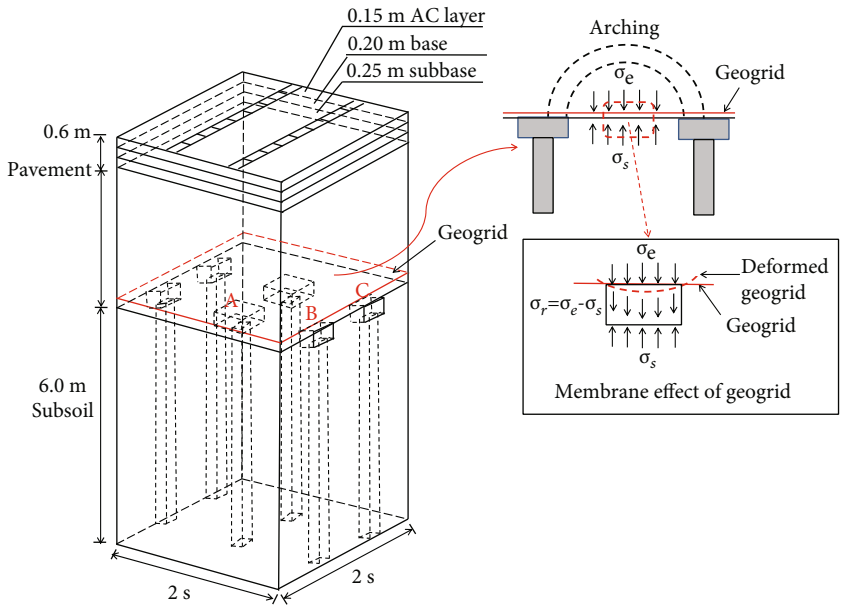

Figure 1: Layout of the reinforced piled embankment.

Table 1: The material parameters used in the finite element analysis.

	h (m)	γ (kN/m^3)	c' (kPa)	φ' (degree)	E (MPa)	Ψ (degree)	μ	λ	κ	M	e_0	e_N	$k_W \times 10^{-4}$ (m/d)
AC layer	0.15	21.0	—	—	4000	—	0.25	—	—	—	—	—	—
Base	0.20	20.0	—	—	1000	—	0.25	—	—	—	—	—	—
Subbase	0.25	18.0	—	—	500	—	0.25	—	—	—	—	—	—
Embankment	2.0, **3.5**, 5.0, 6.5	17.0	**1**, 5, 10	**30**, 35, 40	25	0	0.20	—		—	—	—	—
Pile	6.00	23.5	—	—	30000	—	0.20	—		—	—	—	—
Subsoil	6.00	17.0	—	20	—	—	0.20	0.3	0.1	0.772	1.79	3.44	4.32
Geogrid	Tensile stiffness J = 0, 1, **3**, or 10 MN/m; μ = 0												

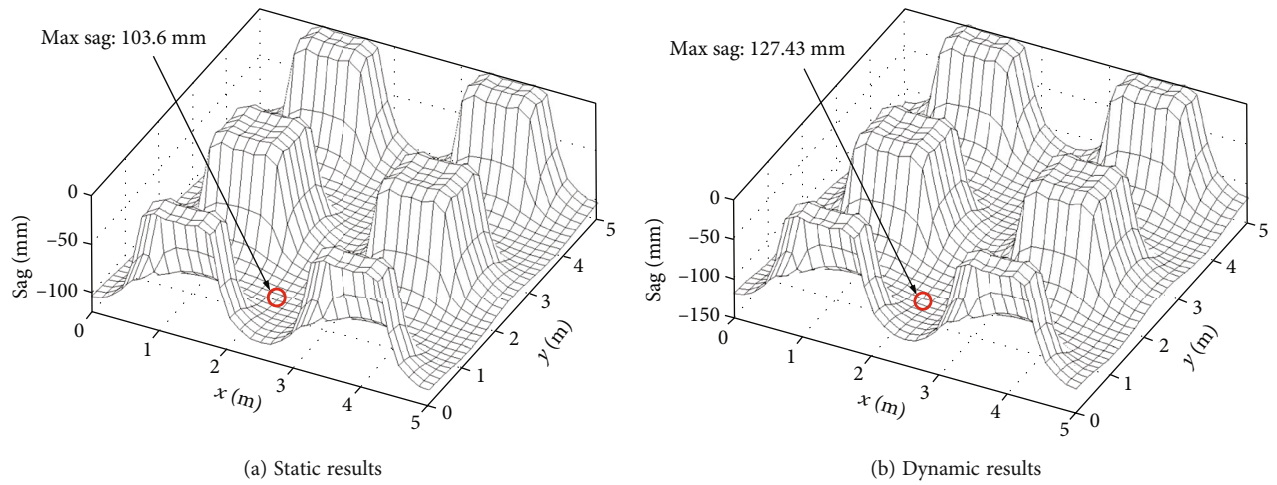

(a) Static results

(b) Dynamic results

Figure 2: Sag of the geogrid (s = 2.5 m, h = 3.5 m, J = 3.0 MN/m, v = 60 km/h).

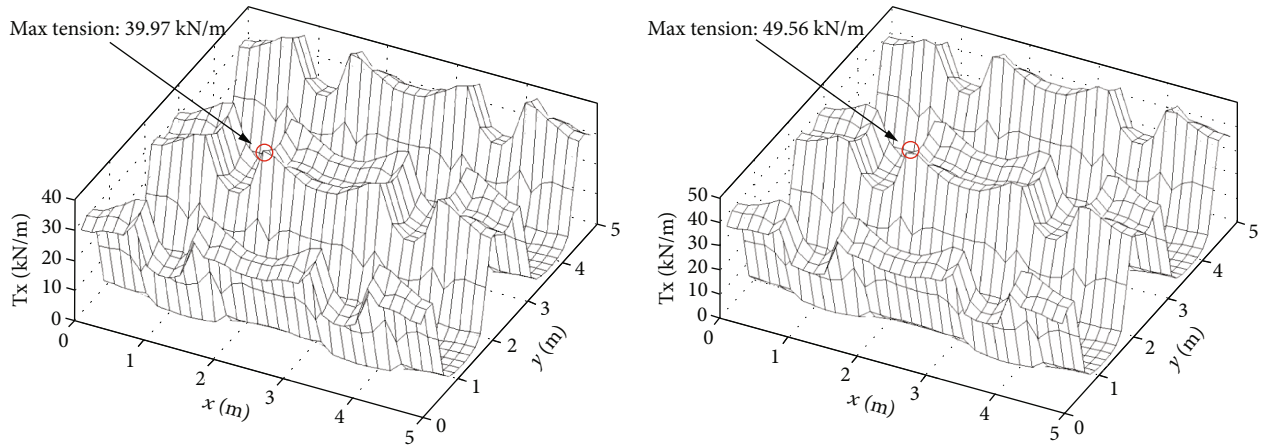

(a) Static results (b) Dynamic results

FIGURE 3: Tensile force of the geogrid along x direction ($s = 2.5$ m, $h = 3.5$ m, $J = 3.0$ MN/m, $v = 60$ km/h).

strain of the geogrid along a horizontal path AB and the diagonal path AC under varied geogrid stiffnesses ($J = 0$ MN/m represents a condition in which the reinforcement is absent, the settlement in Figures 4(a) and 4(b) corresponding to $J = 0$ MN/m is the settlement of the subsoil surface).

The settlements of geogrid are given in Figures 4(a) and 4(b). The deformed shape of the geogrid under static and dynamic loadings under varied geogrid stiffnesses are similar. The settlement at the midpoint of the path AC is slightly greater than that of the path AB. The results are consistent with that reported by Van Eekelen et al. [26, 27] in physical model tests in which the 'inverse triangular load' was imposed on the reinforcement. The maximum settlement under the traffic loading is approximately 23% larger than that under the static loading. What should be mentioned is that the maximum settlement rises once the stiffness of the geogrid decreases. The embankment when the geogrid reinforcement is absent yields the greatest settlement, being approximately 112% larger than that of the standard model.

Figures 4(c) and 4(d) give the strains in the geogrid along with paths AB and AC. Along with the diagonal path AC, the maximum strain is attained at the corner of the pile cap. The strain in geogrid drops to a low magnitude at the center of the path AC. In comparison with the path AC, the strain along path AB is smaller, the distribution of the strain is, however, more uniform than path AC, especially when the geogrid reinforcement with large stiffness is involved.

3.3. Maximum Geogrid Sag and Vertical Stress Acting on Soft Soil. The tensile membrane effect in the piled embankment occurs and simultaneously the soil arching effect develops [6]. Soil arching is quantified to obtain the load acting on the reinforcement (σ_G in Figure 1), while the membrane effect controls the maximum tensile force of the geogrid and thus significantly influences the subsoil settlement. Zhuang et al. [16] demonstrated that the ratio of the height of the embankment to center pile spacing (h/s) is a key design parameter affecting the formation of soil arch. When $h/s \leq 0.5$, there is virtually no soil arching developed. When $0.5 \leq h/s \leq 1.5$, soil arching may partially develop and once $h/s \geq 1.5$ a full soil arching may develop.

Figure 5 illustrates the maximum sag of the geogrid and the maximum vertical stress acting on the soft soil (the midpoint of the path AC) under varied geogrid stiffnesses and h/s. The maximum geogrid sag and the maximum vertical stress acting on the soft soil surface increase when h/s increases and the geogrid stiffness decreases, which may be a result of the coupling effects of soil arching and the tensile membrane effects [6]. It should be mentioned that the pile spacing in Figure 5 keeps constant, i.e., 2.5 m. The value of h/s changes due to the variation of the embankment height. The soil arching enhances with the rise of the embankment height, which significantly affects the load distributed to the piles. The self-weight of the embankment fill becomes larger when its height increases, leading to a rise of the vertical stress at the bottom of the embankment and therefore causing an increase of the maximum strain of reinforcement. When the geogrid is stiffer, the tensile membrane effect improves, which helps the transferring of the vertical stress to the pile caps. The maximum strain of the reinforcement is, therefore, significantly suppressed. The application of the dynamic loading imposes a significant effect on the tensile membrane effect. Under dynamic loading, the maximum sag of the reinforcement approximately increases by 17-46% when compared with the static loading. The application of the dynamic loading causes an increase of around 5-19% on the stress distributed on the soft soil surface.

4. A Comparison of the Geogrid Tensile Force in FE Analysis and Analytical Calculation

A modification was made to the British design code (BS8006) in the year 2010 [8], and thereafter, a further corrigendum was given in 2012 [28]. The 2010 modification incorporated the Hewlett and Randolph model [9] to quantify the soil arching in the piled embankment, while the method was further modified in the 2012 Corrigendum.

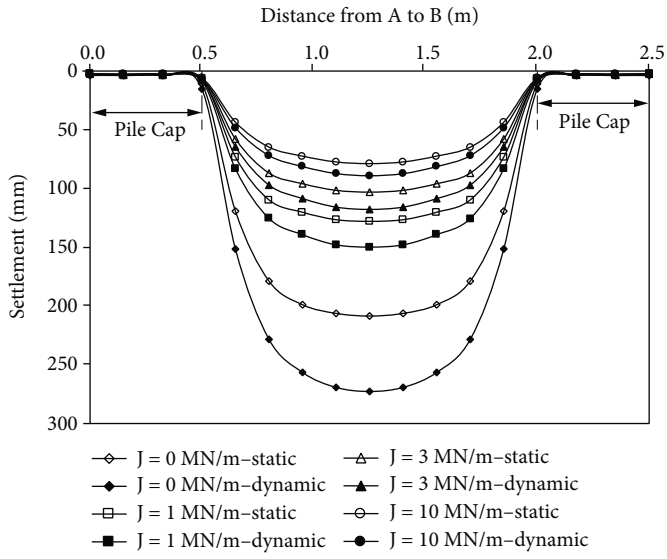

(a) δ from A to B (edge)

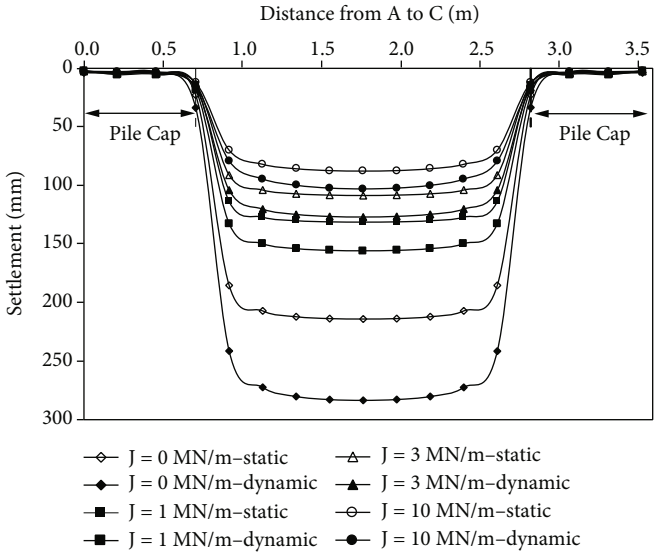

(b) δ from A to C (diagonal)

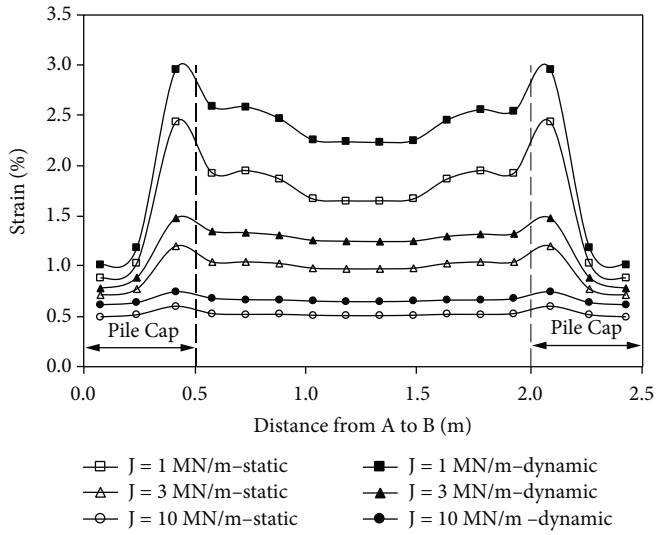

(c) ε from A to B (edge)

Figure 4: Continued.

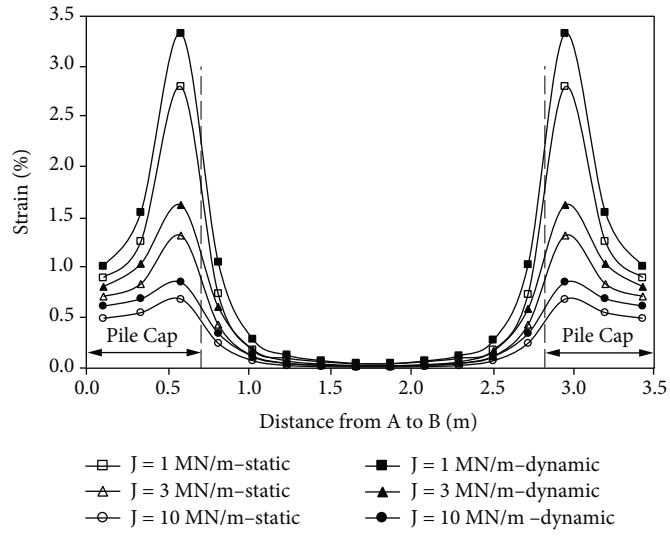

(d) ε from A to C (diagonal)

Figure 4: Settlement (δ) and strain (ε) of geogrid varied with the stiffness ($s = 2.5$ m, $h = 3.5$ m, $v = 60$ km/h).

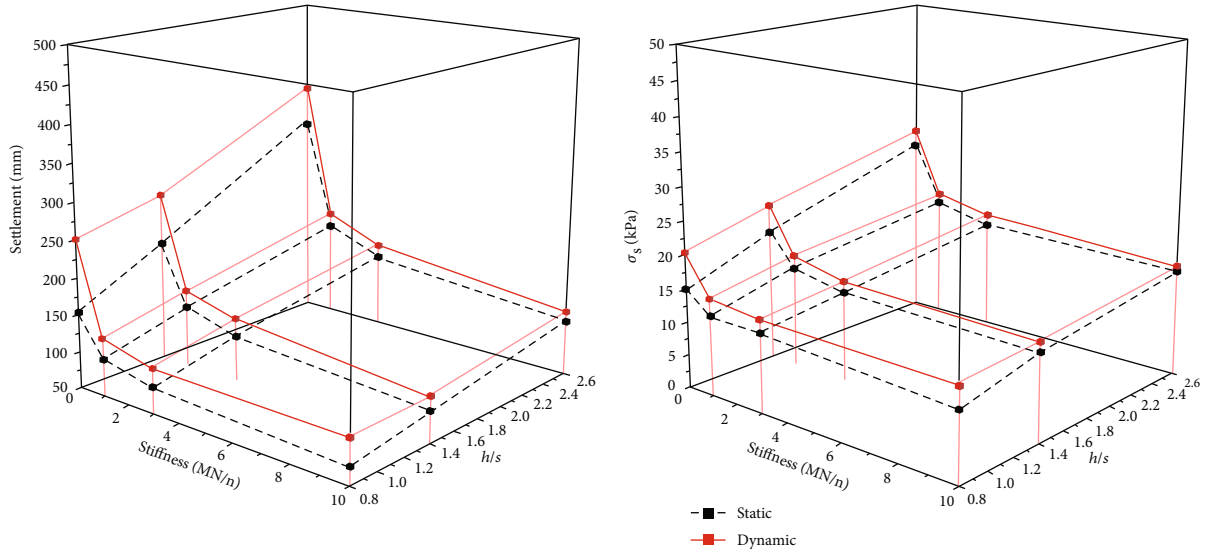

(a) Maximum sag of the geogrid

(b) Maximum vertical stress at the surface of the subsoil

Figure 5: Effect of geogrid stiffness on the maximum geogrid sag and stress distributed at the surface of soft soil over point D.

The two versions of the design code mentioned above adopt the same method to calculate the stress acting on the subsoil surface (σ_s). However, the calculation formulas of the distributed vertical load borne by the reinforcement (W_T) are different from each other, which has been comprehensively investigated by Zhuang and Ellis [12] when the contribution of the subsoil is ignored. Zhuang and Ellis [13] then extend their work by considering the case of lightly overconsolidated soil. By introducing the additional stress caused by the cyclic loadings under the framework of the Boussinesq theory, an analytical solution for the tensile force calculation under dynamic loadings was developed. The detailed formulas can be found in the previously published paper by Zhuang and Wang [23]. The Boussinesq theory is the elastic mechanical solution to the stresses and displacements induced at any point in the half-space when a vertical concentrated force acts on the surface of the elastic half-space.

Figure 6 exhibits the tensile force in the geogrid obtained using the varied method. The lines show the calculated results using the analytical method while the unfilled markers give the results of the FE analysis. In the legend, H&R (2010) and H&R (2012), respectively, represent the Hewlett and Randolph [9] model in the BS80006 for quantifying the soil arching in the version 2010 and the version 2012. NSS and SS, respectively, denote the conditions with no subsoil support and with subsoil support. The detailed formulas can be found in the previously published paper by Zhuang and Ellis [12, 13]. This analysis method gives the calculation of the reinforcement tension with subsoil support without subsoil support, respectively. Figure 6

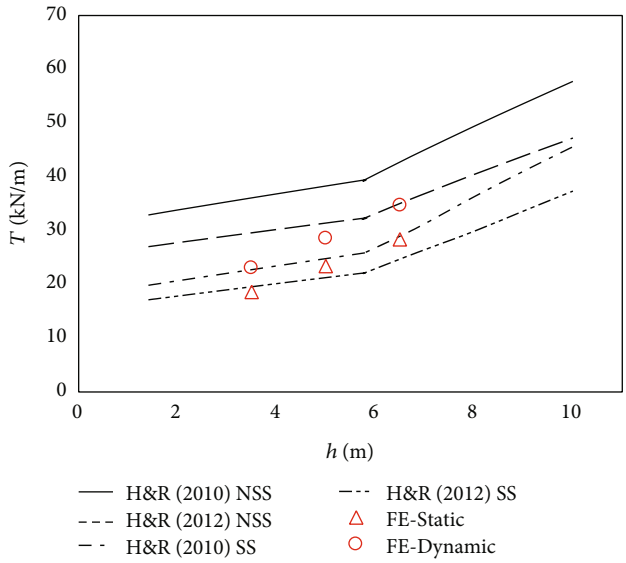

(a) Embankment height ($s = 2.0$ m)

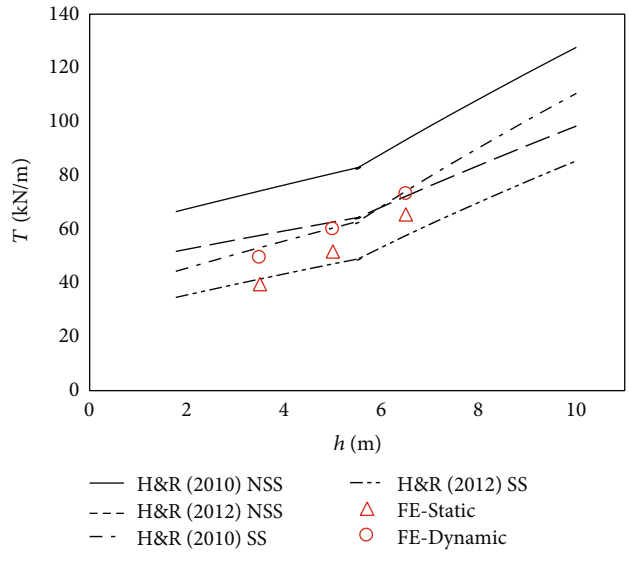

(b) Embankment height ($s = 2.5$ m)

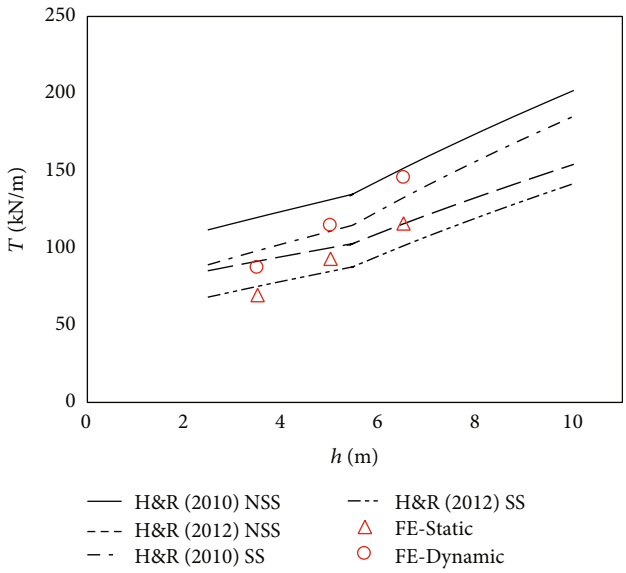

(c) Embankment height ($s = 3.0$ m)

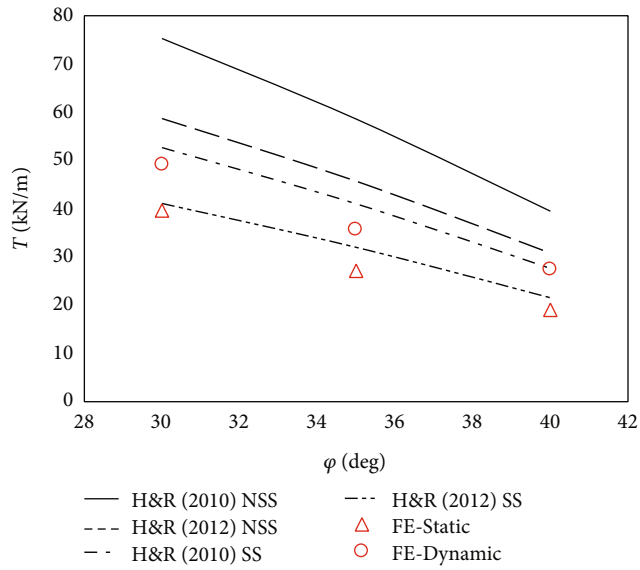

(d) Friction angle of embankment fill

Figure 6: Continued.

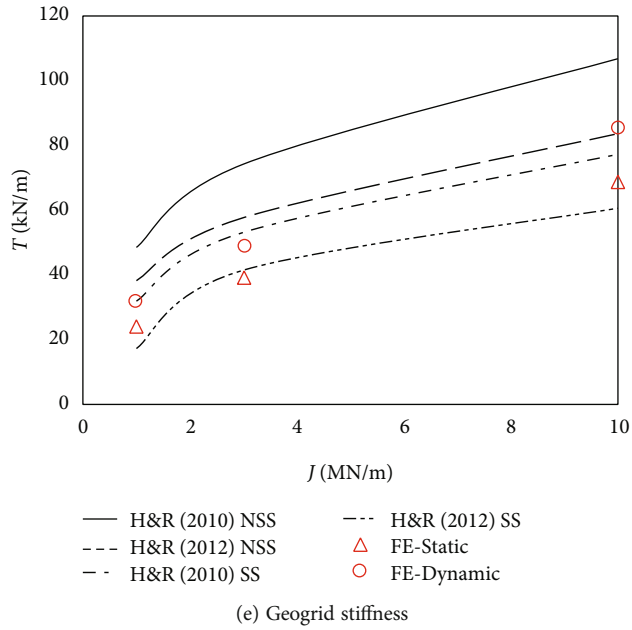

(e) Geogrid stiffness

FIGURE 6: Tensile force of geogrid reinforcement (T) with the change of the influencing factors.

shows the comparison of the numerical results in this study with the calculated results of the analytical method. The results show that the subsoil support decreases the development of the tensile force in the geogrid reinforcement. The tensile force obtained in the FE analysis is about 2%-51% less than the H&R model prediction when the subsoil support is included, while it is around 17%-28% greater than the H&R model prediction once the subsoil support is absent. It can be seen in Figure 6 that the H&R model with subsoil support gives the best prediction of the tensile force in reinforcement when compared with the FE analysis except for a slight underestimation when the embankment height is large. The H&R model without subsoil support roughly overestimates the tensile force mobilized in the reinforcement, which makes its prediction conservative. The tensile force of the geogrid under the dynamic loading remains approximately 11%-45% greater than that under the static loading irrespective of the pile spacing, the friction angle of the embankment, and the tensile stiffness of the geogrid.

It can be seen in Figures 6(a)–6(c) that the tensile force in the geogrid reinforcement rise with the increase of the height of the piled embankment. When the pile spacing is 2.5 m, the tensile force of the geogrid reinforcement approximately increases by 48% when the height of the piled embankment increases from 3.5 m to 6.5 m. The tensile membrane effect shows great sensitivity to the pile spacing. The tensile force in the geogrid increased by 248% once the pile spacing rises from 2.0 m to 3.0 m. The tensile force of the geogrid decreases with the rise of the friction angle of the piled embankment fill. The results showed that the friction angle rising could greatly improve the load transferring of the soil arching. Figure 6(e) shows that the tensile force in geogrid grows with the rise of the tensile stiffness of the geogrid. The tensile force of the geogrid when $J = 3$ MN/m increases by 56% in comparison with that when $J = 1$ MN/m.

5. Conclusions

The study investigated the tensile membrane effect in the geosynthetic reinforced piled embankment under dynamic loading using 3D FE analysis. It has been found that the maximum sag of the geogrid reinforcement was attained at the center between two adjacent piles, while the maximum tension of the geogrid arises at the corners of the pile caps, indicating a significant localization of the geogrid tension. The application of the dynamic loading yields an increase of 45.9% in the sag and 24% in the strain of the geogrid in comparison with the static loading condition.

A parametric study involving the embankment height, the clear pile spacing, the stiffness of reinforcement, and the friction angle of embankment fill was conducted. The result of the FE analysis was also compared with the results obtained from the analytical models, i.e., the H&R model 2010 and 2012 in the BS8006 when the subsoil support was or was not included. When compared with the FE analysis results, the H&R model considering the subsoil support seems to give the best prediction of the tension of the geogrid, while the H&R model ignoring the subsoil support gives a rough overestimation of geogrid tensile force.

The tension of the reinforcement increased with the rise of the clear pile spacing, the embankment height and the geogrid reinforcement stiffness, while it decreased when the embankment fill friction angle increased. The clear pile spacing imposed the greatest effect on the tension of the geogrid reinforcement. The tensile force of the geogrid increased by about 248% when the pile spacing rise from 2.0 m to 3.0 m under dynamic loading.

Data Availability

The data used to support the findings of this study are available from the corresponding author upon request.

Conflicts of Interest

The authors declare that there is no conflict of interest regarding the publication of this paper.

Acknowledgments

The financial supports of the National Natural Science Foundation for Excellent Youth Science Fund Project of China (Grant No. 51922029), the Natural Science Foundation of China (52109139), and the Natural Science Foundation of China General Program (Grant No. 52178316) are acknowledged.

References

[1] A. Johari and A. Talebi, "Stochastic analysis of piled-raft foundations using the random finite-element method," *International Journal of Geomechanics*, vol. 21, no. 4, p. 04021020, 2021.

[2] E. C. A. Fonseca and E. M. Palmeira, "Evaluation of the accuracy of design methods for geosynthetic-reinforced piled embankments," *Canadian Geotechnical Journal*, vol. 56, no. 6, pp. 761–773, 2019.

[3] A. R. Kalantari and A. Johari, "System reliability analysis for seismic stability of the soldier pile wall using the conditional random finite-element method," *International Journal of Geomechanics*, vol. 22, no. 10, p. 04022159, 2022.

[4] T. A. Pham and D. Dias, "3D numerical study of the performance of geosynthetic-reinforced and pile- supported embankments," *Soils and Foundations*, vol. 61, no. 5, pp. 1319–1342, 2021.

[5] D. J. King, A. Bouazza, J. R. Gniel, R. K. Rowe, and H. H. Bui, "Serviceability design for geosynthetic reinforced column supported embankments," *Geotextiles and Geomembranes*, vol. 45, no. 4, pp. 261–279, 2017.

[6] S. J. Feng, S. G. Ai, and H. X. Chen, "Membrane effect of geosynthetic reinforcement subjected to localized sinkholes," *Canadian Geotechnical Journal*, vol. 55, no. 9, pp. 1334–1348, 2018.

[7] E. Ellis and R. Aslam, "Arching in piled embankments: comparison of centrifuge tests and predictive methods," *Ground Engineering*, vol. 42, no. 7, pp. 28–31, 2009.

[8] British Standards Institution, *BS 8006-1: code of practice for strengthened/reinforced soils and other fills*, British Standards Institution, London, UK, 2010.

[9] W. J. Hewlett and M. F. Randolph, "Analysis of piled embankments," *Ground Engineering*, vol. 21, no. 3, pp. 12–18, 1988.

[10] German Geotechnical Society, *Recommendations for design and analysis of earth structures using geosynthetic reinforcements - EBGEO*, German Geotechnical Society, Berlin, Germany, 2011.

[11] S. Hu, Y. Zhuang, X. Zhang, and X. Dong, "A design chart for the analysis of the maximum strain of reinforcement in GRPEs considering the arching and stress history of the subsoil," *Applied Sciences*, vol. 12, no. 5, p. 2536, 2022.

[12] Y. Zhuang and E. Ellis, "Finite-element analysis of a piled embankment with reinforcement compared with BS 8006 predictions," *Geotechnique*, vol. 64, no. 11, pp. 910–917, 2014.

[13] Y. Zhuang and E. A. Ellis, "Finite-element analysis of a piled embankment with reinforcement and subsoil," *Geotechnique*, vol. 66, no. 7, pp. 596–601, 2016.

[14] S. J. M. Van Eekelen, A. Bezuijen, and A. F. Van Tol, "Analysis and modification of the British Standard BS8006 for the design of piled embankments," *Geotextiles and Geomembranes*, vol. 29, no. 3, pp. 345–359, 2011.

[15] S. J. M. Van Eekelen, A. Bezuijen, and A. F. Van Tol, "Validation of analytical models for the design of basal reinforced piled embankments," *Geotextiles and Geomembranes*, vol. 43, no. 1, pp. 56–81, 2015.

[16] Y. Zhuang, K. Y. Wang, and H. L. Liu, "A simplified model to analyze the reinforced piled embankments," *Geotextiles and Geomembranes*, vol. 42, no. 2, pp. 154–165, 2014.

[17] M. S. S. Almeida, D. F. Fagundes, L. Thorel, and M. Blanc, "Geosynthetic-reinforced pile-embankments: numerical, analytical and centrifuge modelling," *Geosynthetics International*, vol. 27, no. 3, pp. 301–314, 2020.

[18] C. Heitz, J. Lüking, and H. G. Kempfert, "Geosynthetic reinforced and pile supported embankments under static and cyclic loading," *European Geosynthetics Conference Eurogeo*, vol. 215, pp. 1–8, 2008.

[19] J. Han and A. Bhandari, "Evaluation of geogrid-reinforced pile-supported embankments under cyclic loading using discrete element method," in *Advances in Ground Improvement*, pp. 73–82, Orlando, Florida, United States, 2009.

[20] R. P. Chen, Y. W. Wang, X. W. Ye, X. C. Bian, and X. P. Dong, "Tensile force of geogrids embedded in pile-supported reinforced embankment: a full-scale experimental study," *Geotextiles and Geomembranes*, vol. 44, no. 2, pp. 157–169, 2016.

[21] H. B. Liu, G. Q. Yang, H. Wang, and B. L. Xiong, "A large-scale test of reinforced soil railway embankment with soilbag facing under dynamic loading," *Geomechanics and Engineering*, vol. 12, no. 4, pp. 579–593, 2017.

[22] Y. Zhuang, X. Cheng, and K. Wang, "Analytical solution for geogrid-reinforced piled embankments under traffic loads," *Geosynthetics International*, vol. 27, no. 3, pp. 249–260, 2020.

[23] Y. Zhuang and K. Y. Wang, "Finite-element analysis of arching in highway piled embankments subjected to moving vehicle loads," *Géotechnique*, vol. 68, no. 10, pp. 857–868, 2018.

[24] J. G. Potyondy, "Skin friction between various soils and construction materials," *Geotechnique*, vol. 11, no. 4, pp. 339–353, 1961.

[25] K. Halvordson, R. Plaut, and G. Filz, "Analysis of geosynthetic reinforcement in pile-supported embankments. Part II: 3D cable-net model," *Geosynthetics International*, vol. 17, no. 2, pp. 68–76, 2010.

[26] S. J. M. Van Eekelen, A. Bezuijen, H. Lodder, and A. F. Van Tol, "Model experiments on piled embankments. Part II," *Geotextiles and Geomembranes*, vol. 32, pp. 82–94, 2012.

[27] S. J. M. Van Eekelen, A. Bezuijen, K. J. Lodder, and A. F. Van Tol, "Model experiments on piled embankments. Part I," *Geotextiles and Geomembranes*, vol. 32, pp. 69–81, 2012.

[28] British Standards Institution, *BS 8006-1: Code of practice for strengthened/reinforced soils and other fills, incorporating corrigendum 1*, British Standards Institution, London, UK, 2012.